Comput. Methods Appl. Mech. Engrg. 198 (2008) 449–458

Contents lists available at ScienceDirect

Comput. Methods Appl. Mech. Engrg.

journal homepage: www.elsevier.com/locate/cma

Coupling finite and boundary element methods for static and dynamic elastic problems with non-conforming interfaces

Thomas Rüberg [a], Martin Schanz [b,*]

[a] Graz University of Technology, Institute for Structural Analysis, Graz, Austria
[b] Graz University of Technology, Institute of Applied Mechanics, Technikerstr. 4, 8010 Graz, Austria

ARTICLE INFO

Article history:
Received 1 February 2008
Received in revised form 4 August 2008
Accepted 26 August 2008
Available online 5 September 2008

Keywords:
FEM–BEM coupling
Linear elastodynamics
Non-conforming interfaces
FETI/BETI

ABSTRACT

A coupling algorithm is presented, which allows for the flexible use of finite and boundary element methods as local discretization methods. On the subdomain level, Dirichlet-to-Neumann maps are realized by means of each discretization method. Such maps are common for the treatment of static problems and are here transferred to dynamic problems. This is realized based on the similarity of the structure of the systems of equations obtained after discretization in space and time. The global set of equations is then established by incorporating the interface conditions in a weighted sense by means of Lagrange multipliers. Therefore, the interface continuity condition is relaxed and the interface meshes can be non-conforming. The field of application are problems from elastostatics and elastodynamics.

1. Introduction

The combination of finite and boundary element methods (FEM and BEM) for the solution of problems arising in structural mechanics is attractive because it allows for an optimal exploitation of the respective advantages of the methods [14,32]. Consider, for instance, the problem of soil-structure interaction, where a finite element method is well-suited for the treatment of the structure and the near-field with its capability of tackling nonlinear phenomena. On the other hand, the finite element mesh has to be truncated which spoils the quality of the numerical analysis especially in dynamics where spurious wave reflections would occur. Boundary element methods are appropriate for the representation of infinite and semi-infinite media and it seems thus natural to employ both methods in combination for such problems.

The idea of combining these two discretization methods goes back to Zienkiewicz et al. [32] who pointed out the complementary characters of the methods and the benefits of their combined use. A mathematical survey of the coupling of FEM and BEM is given by Stephan [29]. One branch of FEM–BEM coupling is the *iterative* coupling in which the individual subdomains are treated independently by either method based on an initial guess of the interface unknowns. Then, the newly computed displacements or tractions on the interface are synchronized and based on these updated values another subdomain solve yields enhanced results. In time domain, this approach is often carried out only once for every time step which gives a staggering scheme. A comprehensive overview of such methods is given by von Estorff and Hagen [5]. Although the iterative coupling is very attractive from the point of software design, the convergence commonly depends on relaxation parameters which are rather empirical [5]. For this reason, a *direct* coupling approach is preferred in this work which is independent of such parameters. Direct FEM–BEM coupling itself can be separated into *substructuring* methods, where the interface conditions are directly fulfilled by setting equal the nodal unknowns, and into *Lagrange multiplier* methods which enforce the interface conditions by auxiliary equations. The substructuring concept for FEM–BEM coupling is given, for instance, in the books of Beer [3] and Hartmann [13]. The drawback of the classical substructuring is that the assembly spoils the structure of the system matrices if, for instance, a sparse symmetric positive definite finite element stiffness matrix and fully-populated nonsymmetric boundary element system matrix are assembled. Moreover, these methods require conforming interface meshes, i.e., the nodes of the interface discretizations have to coincide and the interpolation orders have to be equal on both sides of the interface. The Lagrange multiplier approach circumvents both of the mentioned drawbacks because matrix entries are never mixed from the different subdomains and the interface conditions can be posed in a weighted sense such that non-conforming interfaces can be handled. The mathematical analysis of Lagrange multiplier methods can be found in the book of Steinbach [27] and this concept has been transferred to acoustic-structure coupling by Fischer and Gaul [10]. In this work, a

* Corresponding author. Tel.: +43 316 873 7600.
E-mail address: m.schanz@tugraz.at (M. Schanz).

0045-7825/$ - see front matter © 2008 Elsevier B.V. All rights reserved.
doi:10.1016/j.cma.2008.08.013

Lagrange multiplier approach is preferred because the possibility of combining non-conforming interface discretizations is of great benefit especially when combining finite and boundary elements.

In [11,12], a similar method is proposed for elastostatic problems. But in that approach a three-field method is used. Between the interfaces of two subdomains an additional reference frame with displacement unknowns is introduced. Then, so-called localized Lagrange multipliers between each interface and this frame ensure the coupling conditions. In addition, the Lagrange multipliers are assumed as pointwise constraints in order to avoid the tedious integration over shape functions from different surface discretizations. But the placement of the reference frame degrees of freedom is not straightforward and requires additional work.

In the presented method, the algebraic structure of the final system of equations is similar to the FETI method (see the survey article of Farhat and Roux [9]) and the treatment of floating subdomains is according to [7]. The application of the FETI method to three dimensional elasticity problems especially for the case of large discontinuities in the material parameters is presented in [17]. An extension of the FETI technique to the coupling of finite and boundary element methods is given in [18] which is based on the idea of method-independent Dirichlet-to-Neumann maps. On the other hand, the treatment of non-conforming interface discretizations is well-established within the context of the mortar methods (see the book of Wohlmuth [31]), where special shape functions for the Lagrange multiplier fields are used such that the corresponding unknowns can be eliminated from the final system of equations. The combination of the FETI method with the mortar method has also been carried out in [2] and [25] for the solution of elliptic problems. Here, the concept of the FETI coupling framework for non-conforming interface discretization is followed. It is extended for the employment of boundary element methods as an alternative discretization method and, moreover, carried over to the treatment of dynamic problems in time domain.

The finite element method used in this work is the standard approach for linear elasticity which can be found in the book of Hughes [16]. The employed boundary element method is a collocation approach for static and dynamic problems. See the book of Schanz [24] for a collocation boundary element method for elastodynamic problems. Here, the formulation is slightly altered in order to realize Dirichlet-to-Neumann maps as in [26]. In both cases, i.e., finite and boundary element discretizations, the method itself is not a major point of this work but their combination. Moreover, the established coupling framework is not restricted to the chosen finite and boundary element formulations. Each of the local discretization schemes is easily replaced as long as a Dirichlet-to-Neumann map can be formulated.

2. Linear elastodynamics

2.1. Basic equations

Within the framework of linear elasticity, the dynamics of an elastic solid are governed by the Lamé–Navier equations [1]

$$\frac{\partial^2 \mathbf{u}(\mathbf{x},t)}{\partial t^2} - c_1^2 \nabla(\nabla\cdot\mathbf{u}(\mathbf{x},t)) + c_2^2 \nabla\times(\nabla\times\mathbf{u}(\mathbf{x},t)) = \frac{\mathbf{f}(\mathbf{x},t)}{\rho} \tag{1}$$

in the presence of the body forces $\mathbf{f}(\mathbf{x},t)$. In (1), the vector field $\mathbf{u}(\mathbf{x},t)$ describes the displacement of a material point at point $\mathbf{x}$ and time t. Both the three-dimensional and the plane strain cases are governed by this equation and, therefore, one has $\mathbf{x}\in\mathbb{R}^d$ with $d=2$ or $d=3$ in the following. Moreover, the speeds of the compression and shear wave, c_1 and c_2, are used which are defined by

$$c_1 = \sqrt{\frac{\lambda+2\mu}{\rho}} \quad \text{and} \quad c_2 = \sqrt{\frac{\mu}{\rho}} \tag{2}$$

with the Lamé parameters λ and μ and the mass density ρ. For simplicity, the following shorthand is used for (1)

$$\rho\ddot{\mathbf{u}}(\mathbf{x},t) + (\mathcal{L}\mathbf{u})(\mathbf{x},t) = \mathbf{f}(\mathbf{x},t), \tag{3}$$

where the dot-notation is used for the temporal derivatives and $\mathcal{L}$ is a partial differential operator which is in fact elliptic [28].

The function $\mathbf{u}$ is assumed to have a quiescent past and, therefore, vanishing initial conditions at $t=0$

$$\mathbf{u}(\mathbf{x},0^+) = \dot{\mathbf{u}}(\mathbf{x},0^+) = \mathbf{0}. \tag{4}$$

The boundary trace of the displacement field is denoted by $\mathbf{u}_\Gamma = \mathrm{Tr}\,\mathbf{u}$ and the corresponding traction field by $\mathbf{t} = \mathcal{T}\mathbf{u}$, where Tr is the trace to the boundary Γ and $\mathcal{T}$ is the traction operator. By prescribing boundary conditions on these quantities, an initial boundary value problem is given

$$\begin{aligned} \rho\ddot{\mathbf{u}}(\mathbf{x},t) + (\mathcal{L}\mathbf{u})(\mathbf{x},t) &= f(\mathbf{x},t) \quad (\mathbf{x},t)\in\Omega\times(0,\infty) \\ \mathbf{u}_\Gamma(\mathbf{y},t) &= \mathbf{g}_\mathrm{D}(\mathbf{y},t) \ (\mathbf{y},t)\in\Gamma_\mathrm{D}\times(0,\infty) \\ \mathbf{t}(\mathbf{y},t) &= \mathbf{g}_\mathrm{N}(\mathbf{y},t) \ (\mathbf{y},t)\in\Gamma_\mathrm{N}\times(0,\infty) \end{aligned} \tag{5}$$

together with the initial condition (4). This problem is formulated for the domain Ω with the boundary Γ which is subdivided into the two parts Γ_D and Γ_N where Dirichlet and Neumann boundary conditions are prescribed for the boundary trace $\mathbf{u}_\Gamma$ and the traction $\mathbf{t}$, respectively.

2.2. Variational principle

A possible variational principle for the initial boundary value problem (5) is to require the equation [16]

$$\langle\rho\ddot{\mathbf{u}},\mathbf{v}\rangle + a_t(\mathbf{u},\mathbf{v}) = F_t(\mathbf{v}) \tag{6}$$

to hold for suitably chosen functions $\mathbf{v}$. In this expression, $\langle\mathbf{u},\mathbf{v}\rangle$ is the L_2-scalar product of the displacement field and an admissible test function $\mathbf{v}$. The bilinear form $a_t(\mathbf{u},\mathbf{v})$ is introduced which is defined as

$$a_t(\mathbf{u},\mathbf{v}) = \int_\Omega \boldsymbol{\sigma}(\mathbf{u}) : \boldsymbol{\varepsilon}(\mathbf{v})\,\mathrm{d}\mathbf{x}, \tag{7}$$

where $\boldsymbol{\sigma}(\mathbf{u})$ is the stress tensor due to the displacement field $\mathbf{u}$ and $\boldsymbol{\varepsilon}(\mathbf{v})$ the strain tensor due to the test function $\mathbf{v}$. Moreover, $F_t(\mathbf{v})$ is the linear form

$$F_t(\mathbf{v}) = \int_\Omega \mathbf{f}\cdot\mathbf{v}\,\mathrm{d}\mathbf{x} + \int_{\Gamma_\mathrm{N}} \mathbf{g}_\mathrm{N}\cdot\mathbf{v}_\Gamma\,\mathrm{d}s, \tag{8}$$

where $\mathbf{v}_\Gamma$ is the boundary trace of the test field $\mathbf{v}$. Note that both the bilinear and the linear form carry the subscript t which indicates that they are time dependent.

2.3. Boundary integral equation

Alternatively, the solution $\mathbf{u}$ to the initial boundary value problem (5) can be expressed by the boundary integral representation [24]

$$\begin{aligned} \mathbf{u}(\mathbf{x},t) = &\int_0^t \int_\Gamma \mathbf{U}^*(\mathbf{x}-\mathbf{y},t-\tau)\mathbf{t}(\mathbf{y},\tau)\,\mathrm{d}s_\mathbf{y}\,\mathrm{d}\tau \\ &- \int_0^t \int_\Gamma (\mathcal{T}_\mathbf{y}\mathbf{U}^*(\mathbf{x}-\mathbf{y},t-\tau))^\top \mathbf{u}_\Gamma(\mathbf{y},\tau)\,\mathrm{d}s_\mathbf{y}\,\mathrm{d}\tau. \end{aligned} \tag{9}$$

In this equation, $\mathbf{U}^*(\mathbf{x}-\mathbf{y},t-\tau)$ is the fundamental solution of the Lamé–Navier Eq. (1), see, e.g., [1]. Note that in expression (9) the volume force term $\mathbf{f}$ is assumed to vanish and the material properties are constant throughout the whole domain Ω. Moreover, the integration and the differentiation involved in the application of the traction operator $\mathcal{T}$ to the fundamental solution are with respect to the variable $\mathbf{y}$ which is indicated by the corresponding sub-

scripts. The application of the trace $\mathrm{Tr}_{\mathbf{x}}$ to the integral representation (9) yields the boundary integral equation in operator notation [4]

$$\mathcal{V}_t * \mathbf{t} = \mathcal{C}\mathbf{u}_\Gamma + \mathcal{K}_t * \mathbf{u}_\Gamma, \tag{10}$$

where the asterisk denotes temporal convolution, i.e., $g * h = \int_0^t g(t-\tau)h(\tau)\,\mathrm{d}\tau$. The introduced operators are the single layer operator $\mathcal{V}_t$, the double layer operator $\mathcal{K}_t$, and the integral free term $\mathcal{C}$ which are defined as follows for $\mathbf{x}, \mathbf{y} \in \Gamma$ and $0 < t < \infty$

$$\begin{aligned}
(\mathcal{V}_t * \mathbf{t})(\mathbf{x},t) &= \int_0^t \int_\Gamma \mathbf{U}^*(\mathbf{x}-\mathbf{y},t-\tau)\mathbf{t}(\mathbf{y},\tau)\,\mathrm{d}s_{\mathbf{y}}\,\mathrm{d}\tau,\\
(\mathcal{K}_t * \mathbf{u}_\Gamma)(\mathbf{x},t) &= \lim_{\varepsilon\to 0}\int_0^t \int_{\Gamma_\varepsilon} [(\mathcal{T}_{\mathbf{y}}\mathbf{U}^*(\mathbf{x}-\mathbf{y},t-\tau))^{\mathsf{T}}\mathbf{u}_\Gamma(\mathbf{y},\tau)]\,\mathrm{d}s_{\mathbf{y}}\,\mathrm{d}\tau,\\
(\mathcal{C}\mathbf{u}_\Gamma)(\mathbf{x},t) &= \mathbf{u}_\Gamma(\mathbf{x},t) + \lim_{\varepsilon\to 0}\int_{\gamma_\varepsilon} (\mathcal{T}_{\mathbf{y}}\mathbf{U}^*(\mathbf{x}-\mathbf{y},0))^{\mathsf{T}}\mathbf{u}_\Gamma(\mathbf{x},t)\,\mathrm{d}s_{\mathbf{y}}.
\end{aligned} \tag{11}$$

In these expressions, Γ_ε and γ_ε are integration regions defined by

$$\Gamma_\varepsilon = \Gamma \setminus B_\varepsilon(\mathbf{x}) \quad \text{and} \quad \gamma_\varepsilon = \Omega \cap \partial B_\varepsilon(\mathbf{x}), \tag{12}$$

where the ball of radius ε with center $\mathbf{x}$ is denoted by $B_\varepsilon(\mathbf{x})$ and its surface by $\partial B_\varepsilon(\mathbf{x})$.

2.4. Static case

In the limiting case of a static model, the previously presented equations are simplified. First of all, the boundary value problem is now given by

$$\begin{aligned}
(\mathcal{L}\mathbf{u})(\mathbf{x}) &= \mathbf{f}(\mathbf{x}) \quad \mathbf{x} \in \Omega,\\
\mathbf{u}_\Gamma(\mathbf{y}) &= \mathbf{g}_{\mathrm{D}}(\mathbf{y}) \quad \mathbf{y} \in \Gamma_{\mathrm{D}},\\
\mathbf{t}(\mathbf{y}) &= \mathbf{g}_{\mathrm{N}}(\mathbf{y}) \quad \mathbf{y} \in \Gamma_{\mathrm{N}}
\end{aligned} \tag{13}$$

with the d-dimensional displacement field $\mathbf{u}$ which is now only dependent on the position $\mathbf{x}$. The variational expression (6) reduces to requiring that

$$a(\mathbf{u},\mathbf{v}) = F(\mathbf{v}) \tag{14}$$

holds for all admissible test functions $\mathbf{v}$. Note that the bilinear form $a(\mathbf{u},\mathbf{v})$ and the linear form $F(\mathbf{v})$ do not depend on time anymore and, therefore, the subscript t has been omitted. But their definitions are totally equivalent to (7) and (8). Finally, the static boundary integral equation reads

$$\mathcal{V}\mathbf{t} = \mathcal{C}\mathbf{u}_\Gamma + \mathcal{K}\mathbf{u}_\Gamma \tag{15}$$

with the single and double layer operators $\mathcal{V}$ and $\mathcal{K}$, respectively, which are now defined as

$$\begin{aligned}
(\mathcal{V}\mathbf{t})(\mathbf{x}) &= \int_\Gamma \mathbf{U}^*(\mathbf{x}-\mathbf{y})\mathbf{t}(\mathbf{y})\,\mathrm{d}s_{\mathbf{y}}\\
(\mathcal{K}\mathbf{u}_\Gamma)(\mathbf{x}) &= \lim_{\varepsilon\to 0}\int_{\Gamma_\varepsilon} (\mathcal{T}_{\mathbf{y}}\mathbf{U}^*(\mathbf{x}-\mathbf{y}))^{\mathsf{T}}\mathbf{u}_\Gamma(\mathbf{y})\,\mathrm{d}s_{\mathbf{y}}.
\end{aligned} \tag{16}$$

Of course, in these expressions the fundamental solution $\mathbf{U}^*(\mathbf{x}-\mathbf{y})$ of the operator $\mathcal{L}$ is involved which is independent of time. $\mathbf{U}^*(\mathbf{x}-\mathbf{y})$ is commonly referred to as the Kelvin solution and can be found in [19]. The integral free term $\mathcal{C}$ in (15) is the same as in the definition in (11).

3. Approximation methods

3.1. Finite element method

In order to obtain a finite element scheme, the unknown function $\mathbf{u}$ is approximated by means of the trial [16]

$$\mathbf{u}_h(\mathbf{x},t) = \sum_{i=1}^{I} \varphi_i(\mathbf{x})\mathbf{u}_i(t) \tag{17}$$

with the shape functions φ_i and the time dependent approximation coefficients $\mathbf{u}_i$. Using the test functions $\mathbf{v}$ from the space spanned by the shape functions φ_i and inserting the approximation (17) into the variational formulation (6) yields the system of coupled ordinary differential equations

$$\mathsf{M}\ddot{\mathsf{u}}(t) + \mathsf{A}\mathsf{u}(t) = \mathsf{f}(t). \tag{18}$$

The matrices used in this expression are the mass matrix M, the stiffness matrix A and the force vector f. Moreover, u is the assembly of the time dependent coefficients of the approximation (17) and $\ddot{\mathsf{u}}$ its second time derivative. In fact, one has

$$\begin{aligned}
\mathsf{M}[i,j] &= \langle \rho\varphi_j, \varphi_i\rangle,\\
\mathsf{A}[i,j] &= a_t(\varphi_j,\varphi_i),\\
\mathsf{f}[i] &= F_t(\varphi_i),
\end{aligned} \tag{19}$$

with the bilinear form a_t of (7) and the linear form F_t of (8). The use of a classical time integration scheme such as the Newmark method [22] gives the series of systems of algebraic systems of equations on the equidistant time grid $0 = t_0 < t_1 = \Delta t < \cdots < t_n = n\Delta t$. In any case, this series of equations can be abbreviated by

$$\widetilde{\mathsf{A}}\mathsf{u}_n = \mathsf{f}_n + \mathsf{h}_n \tag{20}$$

with the dynamic stiffness matrix $\widetilde{\mathsf{A}}$, the coefficients of the approximation u_n at time point t_n, the force vector at that time point, and a history term h_n depending on previously computed coefficients of the approximation of the displacement field and possibly of its first and second time derivatives. Note that due to the assumptions of a linear material behavior and the equidistant time grid the left hand side matrix $\widetilde{\mathsf{A}}$ is not altered throughout the computation. In the static case, the system is slightly different, since there is no history term and the dynamic stiffness boils down to the classical stiffness matrix as defined in (19). The resulting system of equation has then the form

$$\mathsf{A}\mathsf{u} = \mathsf{f} \tag{21}$$

with the stiffness matrix A resulting from the static bilinear form a and the force vector f due to the linear form F, both defined similarly to the dynamic versions in (7) and (8).

3.2. Boundary element method

Among the numerous boundary element formulations (see, e.g., [15]) a special collocation method is chosen in this approach. To begin with, the fields of the boundary unknowns $\mathbf{u}_\Gamma$ and $\mathbf{t}$ are approximated by the trials [28]

$$\begin{aligned}
\mathbf{u}_{\Gamma,h}(\mathbf{y},t) &= \sum_{i=1}^{I} \varphi_i(\mathbf{y})\mathbf{u}_i(t),\\
\mathbf{t}_h(\mathbf{y},t) &= \sum_{j=1}^{J} \psi_j(\mathbf{y})\mathbf{t}_j(t)
\end{aligned} \tag{22}$$

with the boundary shape functions φ_i and ψ_j. Now, the $\mathbf{u}_i$ are the coefficients of the boundary displacement field $\mathbf{u}_\Gamma$, not to be confused with the approximation in (17). The shape functions for the unknown $\mathbf{u}_\Gamma$ are piecewise linear continuous functions, whereas the unknown $\mathbf{t}$ is approximated by piecewise linear discontinuous functions. Locating K distinct collocation points $\mathbf{x}_k^*$ on the boundary Γ yields the system of convolution equations

$$(\mathsf{V} * \mathsf{t})(t) = \mathsf{C}\mathsf{u}(t) + (\mathsf{K} * \mathsf{u})(t) \tag{23}$$

with the time dependent matrices resulting from the single and double layer operators defined in (11)

$$\begin{aligned}\mathsf{V}[k,j](t-\tau) &= \int_\Gamma \mathbf{U}^*(\mathbf{x}_k^* - \mathbf{y}, t-\tau)\psi_j(\mathbf{y})\,\mathrm{d}s_\mathbf{y},\\ \mathsf{K}[k,i](t-\tau) &= \lim_{\varepsilon\to 0}\int_{\Gamma_\varepsilon} (\mathcal{T}_\mathbf{y}\mathbf{U}^*(\mathbf{x}_k^* - \mathbf{y}, t-\tau))^\mathsf{T}\varphi_i(\mathbf{y})\,\mathrm{d}s_\mathbf{y}\end{aligned} \tag{24}$$

and the integral free term

$$\mathsf{C}[k,i] = \lim_{\varepsilon\to 0}\int_{\gamma_\varepsilon} (\mathcal{T}_\mathbf{y}\mathbf{U}^*(\mathbf{x}_k^* - \mathbf{y}, 0))^\mathsf{T}\varphi_i(\mathbf{x}_k^*)\,\mathrm{d}s_\mathbf{y}. \tag{25}$$

In both previous expressions, the integration regions Γ_ε and γ_ε are used as defined in (12). Since $\mathbf{U}^*$ is a $d\times d$-matrix, the entries given in Eqs. (24) and (25) are consequently $d\times d$-submatrices of the corresponding system matrices. Note, that the integral free term $\mathcal{C}$ does not depend on time which is accomplished by taking the third and fourth argument of the fundamental solution $\mathbf{U}^*(\mathbf{x}-\mathbf{y}, t-\tau)$ equal as in (25). The remaining convolutions can be discretized by either using the time domain fundamental solution and carrying out the integrations analytically as done, for instance, by Mansur [21] or by using the convolution quadrature method of Lubich [20]. The latter has been transferred to time domain boundary element methods for various materials by Schanz [24] and, in this approach, only the Laplace domain fundamental solution is required by means of which quadrature weights for the convolution integrals are generated. Independent of this choice, the time-discretized version of Eq. (23) has the form

$$\sum_{v=1}^{n}\mathsf{V}_v\mathsf{t}_{n-v} = \mathsf{C}\mathsf{u}_n + \sum_{v=1}^{n}\mathsf{K}_v\mathsf{u}_{n-v} \tag{26}$$

for the time step $t_n = n\Delta t$. The Dirichlet boundary conditions are incorporated by requiring that the approximation (22) directly fulfills those conditions posed on $\mathbf{u}_\Gamma$. By means of the abbreviation

$$\widetilde{\mathsf{K}}_0 = \mathsf{C} + \mathsf{K}_o \quad\text{and}\quad \widetilde{\mathsf{K}}_v = \mathsf{K}_v, \quad 0 < v \leqslant n, \tag{27}$$

the Eq. (26) is converted to

$$\sum_{v=1}^{n}\mathsf{V}_v\mathsf{t}_{n-v} - \sum_{v=1}^{n}\widetilde{\mathsf{K}}_{\mathrm{N},v}\mathsf{u}_{\mathrm{N},n-v} = \sum_{v=1}^{N}\widetilde{\mathsf{K}}_{\mathrm{D},v}\mathsf{g}_{\mathrm{D},n-v}. \tag{28}$$

Here, the subscripts D and N refer to columns of $\widetilde{\mathsf{K}}$ associated with the given Dirichlet and unknown Neumann data, respectively. The approximation of the given Dirichlet datum $\mathbf{g}_\mathrm{D}(t)$ at time point t_n is denoted by $\mathsf{g}_{\mathrm{D},n}$. Similarly, the given Neumann datum $\mathbf{g}_N(t)$ at time point t_n is approximated by $\mathsf{g}_{\mathrm{N},n}$ and is included in a weighted form

$$\mathsf{B}\mathsf{t}_n = \mathsf{B}\mathsf{g}_{\mathrm{N},n} \tag{29}$$

using the mass matrix $\mathsf{B}[i,j] = \langle\psi_j, \varphi_i\rangle$. Note that the vector $\mathsf{g}_{\mathrm{N},n}$ is padded with zeros for coefficients belonging to the Dirichlet boundary Γ_D where this datum is unknown. This corresponds to an extension of the Neumann datum $\mathbf{g}_\mathrm{N}$ with zero to the Dirichlet boundary. The series of systems of equations then reads

$$\begin{pmatrix}\mathsf{V}_0 - \widetilde{\mathsf{K}}_{N,0}\\ \mathsf{B}\end{pmatrix}\begin{pmatrix}\mathsf{t}_n\\ \mathsf{u}_n\end{pmatrix} = \begin{pmatrix}\mathsf{f}_{\mathrm{D},n}\\ \mathsf{f}_{\mathrm{N},n}\end{pmatrix} - \sum_{v=1}^{n}\begin{pmatrix}\mathsf{V}_v - \widetilde{\mathsf{K}}_{\mathrm{N},v}\end{pmatrix}\begin{pmatrix}\mathsf{t}_{n-v}\\ \mathsf{u}_{n-v}\end{pmatrix} \tag{30}$$

with the abbreviations $\mathsf{f}_{\mathrm{D},n} = \widetilde{\mathsf{K}}_{\mathrm{D},n}\mathsf{g}_{\mathrm{D},n}$ and $\mathsf{f}_{\mathrm{N},n} = \mathsf{B}\mathsf{g}_{\mathrm{N},n}$. Using as many collocation points as trial functions for the unknown traction field $\mathbf{t}$, the matrix V_0 becomes quadratic. Note that the use of piecewise constant shape functions for the approximation of the traction field in (22) would result in numerical instabilities in the solution of system (30), see [28].

The static case contains the reduced system of equations

$$\begin{pmatrix}\mathsf{V} - \widetilde{\mathsf{K}}_\mathrm{N}\\ \mathsf{B}\end{pmatrix}\begin{pmatrix}\mathsf{t}\\ \mathsf{u}\end{pmatrix} = \begin{pmatrix}\mathsf{f}_\mathrm{D}\\ \mathsf{f}_\mathrm{N}\end{pmatrix} \tag{31}$$

with the $d\times d$-submatrices of the discretized single and double layer operators

$$\begin{aligned}\mathsf{V}[k,j] &= \int_\Gamma \mathbf{U}^*(\mathbf{x}_k^*, \mathbf{y})\psi_j(\mathbf{y})\,\mathrm{d}s_\mathbf{y}\\ \widetilde{\mathsf{K}}[k,i] &= \mathsf{C}[k,i] + \lim_{\varepsilon\to 0}\int_{\Gamma_\varepsilon}(\mathcal{T}_\mathbf{y}\mathbf{U}^*(\mathbf{x}_k^*, \mathbf{y}))^\mathsf{T}\varphi_i(\mathbf{y})\,\mathrm{d}s_\mathbf{y}\end{aligned} \tag{32}$$

and the integral-free term C similar to (25). Obviously, the force vectors f_D and f_N are defined in the same manner as in the dynamic consideration and the mass matrix B is exactly the same as before.

4. Coupled solution algorithm

4.1. Partitioned problem formulation

The considered mixed initial boundary value problem of linear elastodynamics (5) and the corresponding static case of the mixed boundary value problem (13) are now formulated for a spatial partitioning of the computational domain Ω. For sake of simplicity, at first only the static case of (13) is considered and the extension to dynamic problems is given afterwards.

The domain Ω is subdivided into N_s subdomains $\Omega^{(r)}$, i.e.,

$$\overline{\Omega} = \bigcup_{r=1}^{N_s}\overline{\Omega}^{(r)}, \tag{33}$$

each of which has a boundary $\Gamma^{(r)}$ which is decomposed into a Dirichlet, a Neumann, and an interface part

$$\Gamma^{(r)} = \Gamma_\mathrm{D}^{(r)} \cup \Gamma_\mathrm{N}^{(r)} \cup \left(\bigcup_{p\in J^{(r)}}\Gamma^{(\mathrm{rp})}\right). \tag{34}$$

In this expression, $J^{(r)}$ is the set of indices of subdomains which share an interface with the subdomain $\Omega^{(r)}$. Note that not every subdomain has its share of the Dirichlet and the Neumann boundaries, Γ_D and Γ_N, respectively. In that case, one of the parts $\Gamma_\mathrm{D}^{(r)}$ or $\Gamma_\mathrm{N}^{(r)}$ or both vanish in (34). The mixed boundary value problem for the rth subdomain of the partitioning (33) now reads

$$\begin{aligned}(\mathcal{L}^{(r)}\mathbf{u})(\mathbf{x}) &= \mathbf{f}(\mathbf{x}) \quad \mathbf{x}\in\Omega^{(r)},\\ (\mathrm{Tr}^{(r)}\mathbf{u})(\mathbf{y}) &= \mathbf{g}_\mathrm{D}(\mathbf{y}) \quad \mathbf{y}\in\Gamma_\mathrm{D}^{(r)},\\ (\mathcal{T}^{(r)}\mathbf{u})(\mathbf{y}) &= \mathbf{g}_\mathrm{N}(\mathbf{y}) \quad \mathbf{y}\in\Gamma_\mathrm{N}^{(r)}.\end{aligned} \tag{35}$$

Depending on the geometric constellation of the considered subdomain $\Omega^{(r)}$, the Dirichlet or the Neumann boundary condition is not applicable if the subdomain does not have any share of the corresponding part of the boundary Γ of the original problem. In this boundary value problem, the operators $\mathcal{L}$, Tr, and $\mathcal{T}$ carry the subdomain superscripts in order to emphasize the fact that they can be different for each subdomain. For instance, the material parameters λ, μ, and ρ could vary from subdomain to subdomain. For notational purposes, let $\mathbf{u}^{(r)}$ denote the restriction of the unknown $\mathbf{u}$ to the subdomain $\Omega^{(r)}$ and by Γ_s the skeleton of the partitioning, which is

$$\Gamma_s = \left(\bigcup_{r=1}^{N_s}\Gamma^{(r)}\right)\setminus\Gamma. \tag{36}$$

Problem (35) is not yet completely stated. Therefore, suitable interface conditions have to be formulated in order to embed this local problem into the global constellation. These conditions are commonly the continuity of the displacement field and the equilibrium of the interface tractions

$$\mathbf{u}_\Gamma^{(r)}(\mathbf{y}) = \mathbf{u}_\Gamma^{(p)}(\mathbf{y}), \tag{37a}$$

$$\mathbf{t}^{(r)}(\mathbf{y}) + \mathbf{t}^{(p)}(\mathbf{y}) = \mathbf{0} \tag{37b}$$

for all points $\mathbf{y}$ on the interface $\Gamma^{(rp)}$ and for all such interfaces. Equipping the local mixed boundary value problem (35) with one of the interface conditions (37) yields a well-posed problem. Note that if a subdomain does not have enough share of the global Dirichlet boundary Γ_{D} and only the traction interface condition (37b) is used, its local boundary value problem will not have a unique solution. The displacement field can then be altered by the rigid body motions which are possible due to the lack of prescribed displacements. Such a subdomain is referred to as floating, see also [7] for more details on floating subdomains.

The above considerations are the same for the dynamic case of the initial boundary value problem of linear elastodynamics (5). Therefore, the partitioning and the formulation of local problems is not repeated for this case. Moreover, the same interface conditions (37) have to hold now for all times $t \in (0, \infty)$. Nevertheless, floating subdomains do not appear in dynamics due to the inertia terms in (1).

4.2. Dirichlet-to-Neumann maps

Before the introduction of the coupling strategy, the notion of Dirichlet-to-Neumann maps is presented which enables a coupling formulation independent of the chosen discretization method. Reconsider the boundary integral Eq. (15) which will now be solved for the traction $\mathbf{t}$

$$\mathbf{t} = \underbrace{\mathcal{V}^{-1}(\mathcal{C} + \mathcal{K})}_{\mathcal{S}} \mathbf{u}_\Gamma. \tag{38}$$

Confer [28] for the invertibility of the single layer operator $\mathcal{V}$. The newly introduced operator $\mathcal{S}$ is the so-called Steklov–Poincaré operator [27] and it maps the boundary displacement $\mathbf{u}_\Gamma$ onto the traction $\mathbf{t}$. Eq. (38) is one possible representation of this operator in the continuous setting. It remains to realize this mapping by means of a discretization method.

Reordering the finite element stiffness matrix of (21) according to degrees of freedom associated with the interior of the domain Ω or the boundary Γ yields the system of equation

$$\begin{pmatrix} \mathsf{A}_{II} & \mathsf{A}_{I\Gamma} \\ \mathsf{A}_{\Gamma I} & \mathsf{A}_{\Gamma\Gamma} \end{pmatrix} \begin{pmatrix} \mathsf{u}_I \\ \mathsf{u}_\Gamma \end{pmatrix} = \begin{pmatrix} \mathsf{f}_I \\ \mathsf{f}_\Gamma \end{pmatrix}. \tag{39}$$

The subscripts I and Γ refer to the interior and the boundary degrees of freedom, respectively. The discrete mapping of boundary displacements to boundary nodal forces is now formally established by

$$\underbrace{(\mathsf{A}_{\Gamma\Gamma} - \mathsf{A}_{\Gamma I}(\mathsf{A}_{II})^{-1}\mathsf{A}_{I\Gamma})}_{\mathsf{S}_{\mathrm{fe}}} \mathsf{u}_\Gamma = \underbrace{\mathsf{f}_\Gamma - \mathsf{A}_{\Gamma I}(\mathsf{A}_{II})^{-1}\mathsf{f}_I}_{\mathsf{g}_{\mathrm{fe}}} \tag{40}$$

with the newly introduced abbreviations S_{fe} for the finite element realization of the operator $\mathcal{S}$ and g_{fe} for the boundary forces.

In order to obtain a boundary element realization of this map, simply the first equation of the system (31) is eliminated

$$\underbrace{(\mathsf{BV}^{-1}\widetilde{\mathsf{K}}_{\mathrm{N}})}_{\mathsf{S}_{\mathrm{be}}} \mathsf{u}_\Gamma = \underbrace{\mathsf{f}_{\mathrm{N}} - \mathsf{BV}^{-1}\mathsf{f}_{\mathrm{D}}}_{\mathsf{g}_{\mathrm{be}}}. \tag{41}$$

Now, S_{be} represents the mapping of the boundary displacements u_Γ to the boundary forces g_{be}. Note that in this context the subscript Γ has been added to the unknown coefficients u even in the case of a boundary element method in order to emphasize the structural equivalence between (40) and (41).

In summary, (40) and (41) give possible realizations of the considered Dirichlet-to-Neumann map by means of a finite element or a boundary element discretization. Whereas the former finite element realization is symmetric, the boundary element realization is nonsymmetric. Possible symmetric boundary element discretizations of the operator $\mathcal{S}$ can be found in Refs. [26,27].

Although in dynamics a statement similar to (38) is not available, the above procedure can be repeated exactly in the same manner for the systems (20) and (30). In these cases, the finite element realization of the Dirichlet-to-Neumann map at time point $t_n = n\Delta t$ is

$$\widetilde{\mathsf{S}}_{\mathrm{fe}} \mathsf{u}_{\Gamma,n} = \tilde{\mathsf{g}}_{fe,n} \tag{42}$$

where the following abbreviations have been used

$$\begin{aligned} \widetilde{\mathsf{S}}_{\mathrm{fe}} &= \tilde{\mathsf{A}}_{\Gamma\Gamma} - \tilde{\mathsf{A}}_{\Gamma I}(\tilde{\mathsf{A}}_{II})^{-1}\tilde{\mathsf{A}}_{I\Gamma}, \\ \tilde{\mathsf{g}}_{fe,n} &= \mathsf{f}_{\Gamma,n} + \mathsf{h}_{\Gamma,n} - \widetilde{\mathsf{A}}_{\Gamma I}(\widetilde{\mathsf{A}}_{II})^{-1}(\mathsf{f}_{I,n} + \mathsf{h}_{I,n}). \end{aligned} \tag{43}$$

In case of a dynamic boundary element method, these algebraic manipulations are applied to system (30). This gives the equation

$$\widetilde{\mathsf{S}}_{\mathrm{be}} \mathsf{u}_{\Gamma,n} = \tilde{\mathsf{g}}_{be,n} \tag{44}$$

with the components

$$\begin{aligned} \widetilde{\mathsf{S}}_{\mathrm{be}} &= \mathsf{BV}_0^{-1}\widetilde{\mathsf{K}}_{0N} \\ \tilde{\mathsf{g}}_{\mathrm{be}} &= \mathsf{f}_{\mathrm{N},n} - \mathsf{BV}^{-1}(\mathsf{f}_{\mathrm{D},n} - \ell_n). \end{aligned} \tag{45}$$

For simplicity, the part of the right hand side of system (30) due to the convolution has been abbreviated by ℓ_n, i.e.,

$$\ell_n = \sum_{v=1}^{n} (\mathsf{V}_v \mathsf{t}_{n-v} - \widetilde{\mathsf{K}}_{\mathrm{N},v} \mathsf{u}_{\Gamma,n-v}). \tag{46}$$

Eqs. (42) and (44) thus allow for Dirichlet-to-Neumann maps at each time step using either a finite or a boundary element discretization, respectively.

4.3. FETI framework

By means of the previously presented Dirichlet-to-Neumann maps, the local boundary value problem (35) can be represented by the equivalent boundary-based formulation [27]

$$\begin{aligned} (\mathcal{S}^{(r)}\mathbf{u}_\Gamma^{(r)})(\mathbf{y}) &= \mathbf{g}_\Gamma^{(r)}(\mathbf{y}) \quad \mathbf{y} \in \Gamma^{(r)}, \\ \mathbf{u}_\Gamma^{(r)}(\mathbf{y}) &= \mathbf{g}_{\mathrm{D}}(\mathbf{y}) \quad \mathbf{y} \in \Gamma_{\mathrm{D}}^{(r)}, \\ \mathbf{t}^{(r)}(\mathbf{y}) &= \mathbf{g}_{\mathrm{N}}(\mathbf{y}) \quad \mathbf{y} \in \Gamma_{\mathrm{N}}^{(r)}. \end{aligned} \tag{47}$$

This statement for all subdomains $\Omega^{(r)}$, $1 < r < N_s$, together with the interface conditions (37) represents the global mixed boundary value problem (13). Now, a global variational principle is formulated by incorporating the displacement continuity condition (37a) in a weighted form [27]

$$\begin{aligned} &\int_{\Gamma^{(r)}} (\mathcal{S}^{(r)}\mathbf{u}_\Gamma^{(r)}) \cdot \mathbf{v}_\Gamma^{(r)} \,\mathrm{d}s + \sum_{p \in J^{(r)}} \int_{\Gamma^{(rp)}} \boldsymbol{\lambda}^{(rp)} \cdot (\mathbf{v}_\Gamma^{(r)} - \mathbf{v}_\Gamma^{(p)}) \,\mathrm{d}s = \int_{\Gamma^{(r)}} \mathbf{g}_\Gamma^{(r)} \cdot \mathbf{v}_\Gamma^{(r)} \,\mathrm{d}s \\ &\sum_{p \in J^{(r)}} \int_{\Gamma^{(rp)}} \boldsymbol{\mu}^{(rp)} \cdot (\mathbf{u}_\Gamma^{(r)} - \mathbf{u}_\Gamma^{(p)}) \,\mathrm{d}s = 0. \end{aligned} \tag{48}$$

These two expressions have to hold for subdomains $\Omega^{(r)}$. For the weighted formulation of the interface conditions a Lagrange multiplier field $\boldsymbol{\lambda}$ has been introduced on the skeleton Γ_s of the partitioning, where $\boldsymbol{\lambda}^{(rp)}$ denotes its restriction to the interface $\Gamma^{(rp)}$. Moreover, the functions $\mathbf{v}_\Gamma^{(r)}$ and $\boldsymbol{\mu}^{(rp)}$ are the test functions which correspond to the fields of the local boundary displacement $\mathbf{u}_\Gamma^{(r)}$ and the Lagrange multiplier $\boldsymbol{\lambda}^{(rp)}$, respectively.

Using the framework of the FETI method of Refs. [8,9], the discretized version of the variational form (48) is

$$\begin{pmatrix} \mathsf{S}^{(1)} & & & & \mathsf{C}^{(1)\mathsf{T}} \\ & \mathsf{S}^{(2)} & & & \mathsf{C}^{(2)\mathsf{T}} \\ & & \ddots & & \vdots \\ & & & \mathsf{S}^{(N_s)} & \mathsf{C}^{(N_s)\mathsf{T}} \\ \mathsf{C}^{(1)} & \mathsf{C}^{(2)} & \cdots & \mathsf{C}^{(N_s)} & \end{pmatrix} \begin{pmatrix} \mathsf{u}_\Gamma^{(1)} \\ \mathsf{u}_\Gamma^{(2)} \\ \vdots \\ \mathsf{u}_\Gamma^{(N_s)} \\ \lambda \end{pmatrix} = \begin{pmatrix} \mathsf{g}_\Gamma^{(1)} \\ \mathsf{g}_\Gamma^{(1)} \\ \vdots \\ \mathsf{g}_\Gamma^{(N_s)} \\ 0 \end{pmatrix}. \tag{49}$$

In this system, the matrices $\mathsf{S}^{(r)}$ represent the local discretizations of the operator $\mathcal{S}^{(r)}$ and can be either a finite element or a boundary element realization according to (40) or (41), respectively. The boundary force vectors $\mathsf{g}_\Gamma^{(r)}$ result from the same considerations. The matrices $\mathsf{C}^{(r)}$ are the discretizations of the terms corresponding to the interface conditions of the variational expression (48) and will be henceforth referred to as connectivity matrices. Finally, the vector λ gathers the coefficients of suitable approximation of the Lagrange multiplier field $\boldsymbol{\lambda}$. This approximation will be discussed in more detail below. In dynamic problems, exactly the same system of equations results at each time step. Then the left and right hand sides have to be replaced by the finite element matrices of (43) or the boundary element matrices of (45).

In order to solve system (49), at first it is assumed that the matrices $\mathsf{S}^{(r)}$ are invertible. Then, the local boundary displacements are given by

$$\mathsf{u}_\Gamma^{(r)} = \mathsf{S}^{(r)\,-1}(\mathsf{g}_\Gamma^{(r)} - \mathsf{C}^{(r)\,\mathsf{T}}\lambda). \tag{50}$$

Inserting this expression into the last line of the system (49), yields the equation for the Lagrange multiplier coefficients

$$\underbrace{\sum_{r=1}^{N_s} \mathsf{C}^{(r)}\mathsf{S}^{(r)\,-1}\mathsf{C}^{(r)\,\mathsf{T}}}_{\mathsf{F}}\lambda = \underbrace{\sum_{r=1}^{N_s} \mathsf{C}^{(r)}\mathsf{S}^{(r)\,-1}\mathsf{g}_\Gamma^{(r)}}_{\mathsf{d}}. \tag{51}$$

In case of dynamic problems, the regularity of expression (50) is guaranteed. But in the static case, the matrix $\mathsf{S}^{(r)}$ has no unique inverse if the subdomain $\Omega^{(r)}$ is floating. Then a so-called generalized inverse and the null-space of the matrix are needed in order to give the local boundary displacements

$$\mathsf{u}_\Gamma^{(r)} = \mathsf{S}^{(r)+}(\mathsf{g}_\Gamma^{(r)} - \mathsf{C}^{(r)\,\mathsf{T}}\lambda) + \mathsf{N}^{(r)}\alpha^{(r)}. \tag{52}$$

The generalized inverse is denoted by the superscript + and $\mathsf{N}^{(r)}$ is the null-space of $\mathsf{S}^{(r)}$, i.e., $\mathsf{S}^{(r)}\mathsf{N}^{(r)} = 0$. Moreover, the vector $\alpha^{(r)}$ collects the amplitudes of the rigid body motions of the subdomain. Here, the procedure described in [7] is adopted which yields a robust scheme for the computation of both the generalized inverse and the null-space of a rank-deficient matrix. Expression (52) introduces another field of unknowns α and, therefore, more equations are required. The local solvability condition reads [9]

$$\mathsf{N}_R^{(r)\,\mathsf{T}}(\mathsf{g}_\Gamma^{(r)} - \mathsf{C}^{(r)\,\mathsf{T}}\lambda) = 0, \tag{53}$$

with the right null-space $\mathsf{N}_R^{(r)}$ of $\mathsf{S}^{(r)}$, i.e., $\mathsf{N}_R^{(r)\,\mathsf{T}}\mathsf{S}^{(r)} = 0$. Due to the symmetry of the finite element realization $\mathsf{S}_{\mathrm{fe}}^{(r)}$, the right and left null-spaces, $\mathsf{N}_R^{(r)}$ and $\mathsf{N}^{(r)}$, coincide. In case of the nonsymmetric boundary element realization $\mathsf{S}_{\mathrm{be}}^{(r)}$, this symmetry is assumed here based on the fact that both matrices represent the same physical characteristics.

Inserting expression (52) into the last line of system (49) and assembling the solvability conditions (53) for all subdomains finally gives the system of equations

$$\begin{pmatrix} \mathsf{F} & -\mathsf{G} \\ -\mathsf{G}^{\mathsf{T}} & \end{pmatrix}\begin{pmatrix} \lambda \\ \alpha \end{pmatrix} = \begin{pmatrix} \mathsf{d} \\ -\mathsf{e}^{\mathsf{T}} \end{pmatrix}. \tag{54}$$

In addition to the quantities F and d due to expression (51), there are the matrices

$$\begin{aligned} \mathsf{G} &= (\mathsf{C}^{(1)}\mathsf{N}^{(1)}, \ldots, \mathsf{C}^{(N_s)}\mathsf{N}^{(N_s)}) \\ \mathsf{e} &= (\mathsf{N}^{(1)\,\mathsf{T}}\mathsf{g}_\Gamma^{(1)}, \ldots, \mathsf{N}^{(N_s)\,\mathsf{T}}\mathsf{g}_\Gamma^{(N_s)}). \end{aligned} \tag{55}$$

The original FETI method due to [8] has been tailored for finite element discretizations of static problems and is equipped with projected conjugate gradient solver for an optimally parallelized solution procedure. Such concepts have been transferred to dynamic problems in [6]. Nevertheless, the development of fast iterative solution procedures is here not the principal aim and left as future research. Especially, the lack of symmetry due to the chosen boundary element formulation and, therefore, of the matrix F would require a lot more effort in the design of such a solver. Therefore, direct solution routines are used for both the static and dynamic problems considered here.

4.4. Connectivity matrices

In the original FETI algorithm [8], the Lagrange multipliers are used as node-wise constraints. Therefore, the connectivity matrices are just such that $\mathsf{C}[j,i] \in \{0, 1, -1\}$. This simple and efficient approach implies conforming interface discretizations, i.e., the nodes of adjacent subdomains have to spatially coincide at their common interface and, moreover, the polynomial orders of the local discretizations have to be equal. In such a case, the interface condition (37a) is fulfilled exactly at every point of the interface. Here, this requirement shall be relaxed and non-conforming interfaces are allowed. Therefore, the introduced Lagrange multiplier field is approximated by

$$\boldsymbol{\lambda}_h(\mathbf{y}) = \sum_{j=1}^{N_\lambda} \psi_j(\mathbf{y})\boldsymbol{\lambda}_j \tag{56}$$

with the shape functions ψ_j and the approximation coefficients $\boldsymbol{\lambda}_j$. By means of this approximation, the connectivity matrices become

$$\mathsf{C}^{(r)}[j,i] = \pm\int_{\bigcup} \varphi_i^{(r)}(\mathbf{y})\psi_j(\mathbf{y})\,\mathrm{d}s. \tag{57}$$

In this expression, $\varphi^{(r)}$ refers to a boundary element function for the approximation of $\mathbf{u}_\Gamma^{(r)}$ or to the boundary trace of a finite element function for the approximation of $\mathbf{u}^{(r)}$. The integration is carried out over all interfaces of the considered subdomain $\Omega^{(r)}$ as indicated by the union in the integration limit. The sign is adjusted such that at adjacent sides of the interface it becomes opposite. For instance, one can assume the convention that if $p < r$ the sign in (57) is positive and it is negative for $r < p$. Note that if the shape functions ψ_j are taken to be Dirac delta distributions, i.e., $\psi_j(\mathbf{y}) = \delta(\mathbf{y} - \mathbf{x}_j)$ with $\mathbf{x}_j$ being the jth interface node, then (57) reduces to the classical FETI connectivity matrices.

In order to establish a non-conforming coupling, let at any interface $\Gamma^{(rp)}$ for $r < p$ the subdomain $\Omega^{(r)}$ be the slave and $\Omega^{(p)}$ be the master as in the mortar method [31]. This indicates that the approximation of the Lagrange multiplier field (56) is defined with respect to the interface mesh inherited from the slave side. With this arbitrary convention, the interface matrices obtain the contributions at the interface $\Gamma^{(rp)}$

$$\begin{aligned} \Omega^{(r)} &: \mathsf{C}^{(r)}[i,j] = -\int_{\Gamma^{(rp)}} \varphi_i^{(r)}(\mathbf{y})\psi_j^{(r)}(\mathbf{y})\,\mathrm{d}s \\ \Omega^{(p)} &: \mathsf{C}^{(p)}[k,j] = +\int_{\Gamma^{(rp)}} \varphi_k^{(p)}(\mathbf{y})\psi_j^{(r)}(\mathbf{y})\,\mathrm{d}s. \end{aligned} \tag{58}$$

The first of these contributions is again of the standard mass-matrix type but in the second contribution $\mathsf{C}^{(p)}[k,j]$ the difficulty occurs that the L_2-product of two shape functions is performed which are defined on different meshes.

For sake of simplicity, the shape functions $\psi_j(\mathbf{y})$ are assumed piecewise constant. Then, the second and crucial expression in (58) becomes

$$\mathsf{C}^{(p)}[k,j] = +\int_{\tau_j^{(r)}} \varphi_k^{(p)}(\mathbf{y})\,\mathrm{d}s \tag{59}$$

with the element $\tau_j^{(r)}$ associated with the shape function $\psi_j^{(r)}$ of the interface discretization of subdomain $\Omega^{(r)}$. The interfaces $\Gamma^{(rp)}$ are assumed to be flat such that for any discretization of the adjacent subdomains the computational representations of the geometry cannot overlap or form voids. The first step in the computation of

the value of $c^{(p)}[k,j]$ is to determine the overlap of the element $\tau_j^{(r)}$ of subdomain $\Omega^{(r)}$ with the support of the shape function $\varphi_k^{(p)}$. Hence, one has to find the intersection

$$\bar{\tau}_{kj}^{(rp)} = \tau_j^{(r)} \cap \mathrm{supp}(\varphi_k^{(p)}). \tag{60}$$

This task is trivial in case of a two-dimensional analysis, where only the intersection of one-dimensional intervals has to be computed. Contrary to this, in a three-dimensional analysis the geometric overlap of two-dimensional surface elements has to be determined. Therefore, the elements of the master domain $\Omega^{(p)}$ are transformed to the reference space of the slave domain $\Omega^{(p)}$ and then the techniques of polygon clipping are used as described in [30]. Once the region $\bar{\tau}_{kj}^{(rp)}$ is computed a quadrature rule is applied to the integral of (59). Since the computed overlap is a convex polygon of rather arbitrary shape, it will thus be subdivided into triangles on each of which a quadrature rule is carried out. In this context, another difficulty appears because the shape function $\varphi_k^{(p)}$ is defined with respect to the reference elements of subdomain $\Omega^{(p)}$ and, therefore, its evaluation at quadrature points expressed in the reference space of the slave subdomain $\Omega^{(r)}$ is not straightforward. Suitable coordinate transformations between these space are required as pointed out in [23].

Once the connectivity matrices are computed according to the above described procedure, the FETI solution process can be carried out as in the original algorithm of [8]. The only difference is that in the original FETI algorithm only extraction procedures are required due to the simple structure of the matrices $\mathsf{C}^{(r)}$, whereas the procedure described here requires floating point arithmetic for the matrix–matrix products in (51) and (55). On the other side, so-called cross points, that are points at which more than two subdomains meet, do not pose any problem in this approach. The Lagrange multiplier field is associated with elements and not with nodes and, therefore, the multipliers cannot be redundant. Note that the case of conforming interface discretizations is fully included in this approach and would yield equal expressions for the contributions in (58).

5. Numerical examples

The approximations for the following examples are all of the following type. For the finite element discretizations bilinear quadrilaterals or trilinear hexahedra elements are used in two or three dimensions, respectively. The boundary element analysis is based on piecewise linear shape functions which are continuous for the boundary displacements $\mathbf{u}_\Gamma$ and discontinuous for the tractions $\mathbf{t}$. In two dimensions simple line elements are used and in three dimensions triangular elements. The mesh sizes h refer either to the length of the sides of the quadrilaterals or hexahedra, the length of the line elements or the catheti of the triangles. For the time discretization of the dynamic finite element method the Newmark algorithm with parameters $\beta = 0.25$ and $\gamma = 0.5$ is taken. This choice corresponds to an unconditionally stable scheme with second order accuracy and without numerical dissipation [16].

5.1. Static analysis of a cantilever beam

The first test case to consider is the numerical analysis of a cantilever beam by means of the presented coupling approach. Therefore, a domain of dimensions 10 m × 1 m × 1 m is considered as a representation of the cantilever beam. The beam is fixed at $x_1 = 0$, which is the given Dirichlet datum, i.e., $\mathbf{g}_\mathrm{D} = \mathbf{0}$. The opposite side at $x_1 = 10$ m is subjected to a vertical uniformly distributed load with the non-zero component $\mathbf{g}_\mathrm{N} = -1\ \mathrm{N/m^2}\ \mathbf{e}_3$. Every other part of the surface Γ is traction free. The material is assumed to be steel without any lateral contraction having the material parameters $\lambda = 0$ and $\mu = 1.055 \times 10^{11}\ \mathrm{N/m^2}$.

A two- and a three-dimensional analysis are carried out where the domain Ω is subdivided into four subdomains $\Omega^{(r)}$, $r = 1, \ldots, 4$. Each of these subdomains is of equal size and has the dimensions 5 m × 1 m × 0.5 m and the constellation is shown in Fig. 1 together with the numbering of the subdomains.

In the numerical analysis, subdomains $\Omega^{(1)}$ and $\Omega^{(4)}$ are always treated by the same discretization method with the same mesh size and so are subdomains $\Omega^{(2)}$ and $\Omega^{(3)}$. The three combinations of coupling boundary with boundary elements (BEM–BEM), boundary with finite elements (BEM–FEM), and finite with finite elements (FEM–FEM) are considered. Each of these cases is treated with a coarse, a middle, and a fine discretization. The mesh widths are given in Table 1 and an example of these discretizations is shown in Fig. 2 where the case BEM–FEM for the middle mesh is displayed.

In order to judge the numerical outcome of the different analyses, the results of a finite element solution with the whole cantilever beam as one domain is used as a reference solution $\mathbf{u}_\mathrm{ref}$. This finite element solution is obtained with $h = 1/40$ m for the two-dimensional and $h = 1/20$ m for the three-dimensional analysis, respectively. An error measure is defined by considering the value of

$$\varepsilon(x_1) = \frac{|u_3(x_1,0,0) - u_{\mathrm{ref},3}(x_1,0,0)|}{|u_{\mathrm{ref},3}(x_1,0,0)|}, \tag{61}$$

where u_3 denotes the vertical displacement of the numerical analysis of the centerline at $x_2 = x_3 = 0$ and $u_{\mathrm{ref},3}$ is the vertical component of the reference solution $\mathbf{u}_\mathrm{ref}$.

In Fig. 3, the outcome of the numerical analysis with the various combinations described above is plotted in terms of the error measure defined in (61). Obviously, the results of the two-dimensional BEM–BEM coupling are worse than the other combinations. The BEM–FEM combination performs better and the best results are given by the FEM–FEM coupling. On the other hand, in the three-dimensional analysis the order of the quality of the results is reversed. Here, the BEM–BEM coupling yields better results than the other combinations and the FEM–FEM coupling has the worst performance. Concentrating on the results closer to the loaded end of the beam, one can see that in all coupling combinations the results improve with finer discretizations. A closer look at the outcome of the three-dimensional analysis in Fig. 3 reveals small discontinuities in the curves at $x_1 = 5$ m. This effect can be explained by the weak statement of the displacement continuity

Table 1
Different discretizations of the cantilever problem

Mesh	$h^{(1)} = h^{(4)}$	$h^{(2)} = h^{(3)}$
Coarse	1/6 m	1/4 m
Middle	1/6 m	1/8 m
Fine	1/10 m	1/8 m

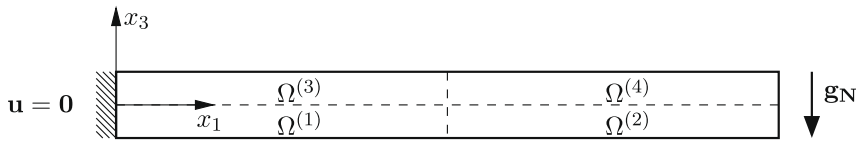

Fig. 1. Model of cantilever beam with four subdomains.

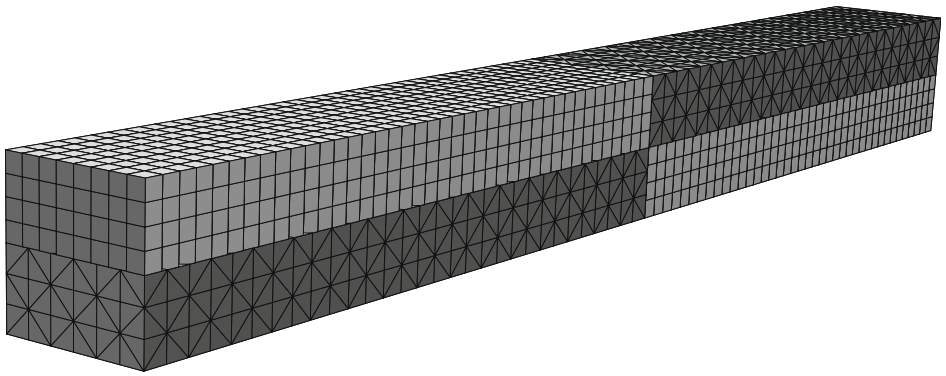

Fig. 2. Discretization of the three-dimensional model of the cantilever beam with finite and boundary elements.

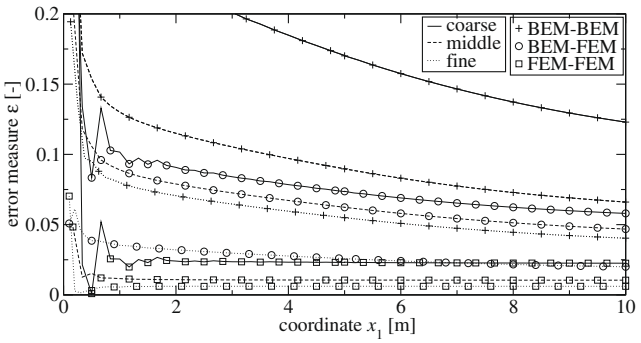

(a) Two-dimensional analysis.

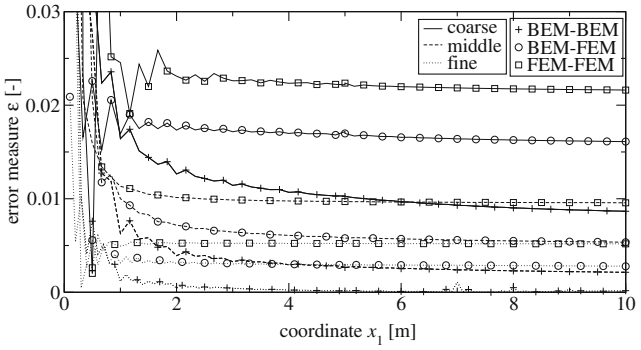

(b) Three-dimensional analysis.

Fig. 3. Results of the coupled analysis of the cantilever beam — error measure according to (61) along the coordinate x_1 for the various considered combinations in two and three dimensions.

condition (37a) and, obviously, it does not deteriorate the results away from the interface.

5.2. Unit step load on a rod

As a dynamic test case, an elastic rod which is fixed at one end and subject to a unit step load at the other end is considered. The problem is depicted in Fig. 4, where a rod of length ℓ is shown with a fixed left end at $x_1 = 0$ and the longitudinal step load $F_0 H(t)$ is applied at the right end at $x_1 = \ell$. Here, $H(t)$ is the Heaviside function, i.e., $H(t) = 0$ for $t \leqslant 0$ and $H(t) = 1$ for $t > 0$. The analytical solution of the problem is given, for instance, in [24]. Here, again the material steel is used with the parameters $\lambda = 0$, $\mu = 1.055 \times 10^{11}$ N/m^2, and $\rho = 7850$ kg/m^3. The other parameters are the length of the rod with the value $\ell = 3$ m and the magnitude of the load $F_0 = 1$ N.

The domain of dimensions 3 m × 1 m × 1 m is subdivided into three unit cubes. The first and the third of which are discretized by the boundary element method with a mesh width of $h^{(1)} = h^{(3)} = 0.25$ m. The middle cube is discretized by finite elements with $h^{(2)} = 0.5$ m for a coarse and $h^{(2)} = 0.2$ m for a fine discretization. The constellation with the fine discretization is shown in Fig. 5.

The choice of the time step size has been determined according to stability conditions of the convolution quadrature method of the dynamic boundary element method. Such considerations can be found in detail in [24] and lead to the observation that the size of the time step is bounded from below. As in other time discretization methods, the ratio $\beta = (c_1 \Delta t)/h$ is fundamental for stability analyses. According to [24] this value is here fixed to approximately $\beta = 0.2$ which corresponds to a time step size of $\Delta t = 10^{-6}$ s.

In the numerical analysis, the longitudinal displacements u_1 along the middle axis are considered at the loaded face and the interfaces. Moreover, the traction component t_1 at the fixed end is regarded. Therefore, the points A, B, and C refer to the coordinates $x_1 = 3$ m, $x_1 = 2$ m, and $x_1 = 1$ m, respectively along this middle axis, i.e., at $x_2 = x_3 = 0.5$ m. These coordinates correspond to the coordinate system in Fig. 4 if placed along the centerline of the cuboid domain. The outcome is plotted in Fig. 6 together with the analytical solution. The numerical solution for the displacements reproduces well the zigzag curve of the analytical solution. Especially, the finer discretization yields results which are hardly distinguishable from the analytical solution. The traction solution of the coarse discretization deviates significantly from the analytical solution. Nevertheless considering the fact that a discontinuous function is approximated, the results for the fine discretization are reasonably good despite the overshoots at each jump.

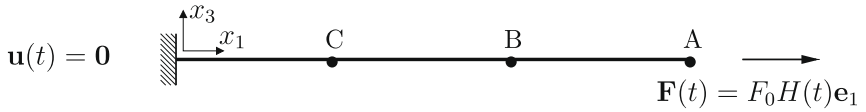

Fig. 4. Rod with a unit step force. Displacement results are considered for the points A, B, and C.

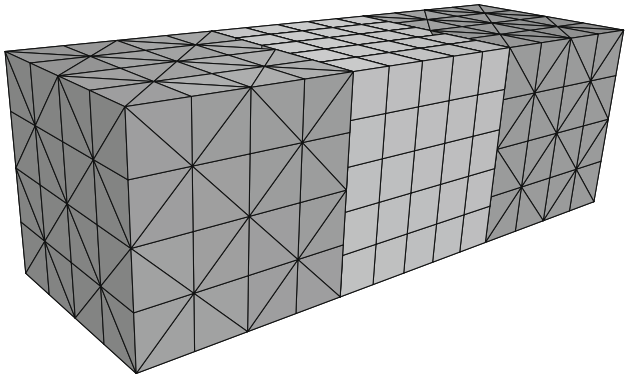

Fig. 5. Boundary element and finite element discretization of the dynamic loaded rod.

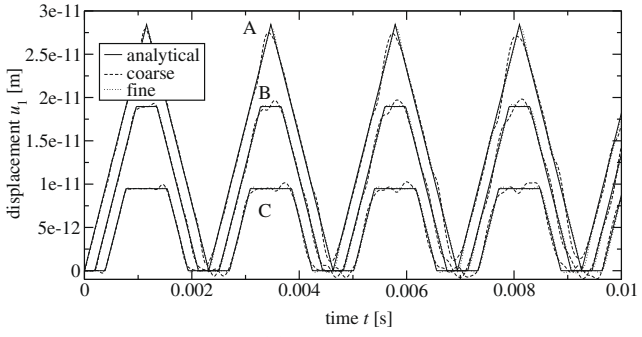

(a) Displacements.

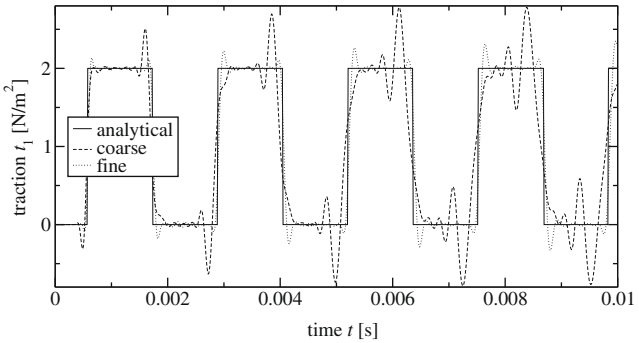

(b) Tractions.

Fig. 6. Coupled boundary and finite element solution for the three-dimensional rod – displacements at points A, B, and C and traction at the fixed end against time.

5.3. Foundation on an elastic halfspace

Finally, the static and dynamic analyses of an individual footing on an elastic halfspace is considered. The foundation is assumed to be of cuboid shape and made of concrete with parameters $\lambda = 9.72 \times 10^9$ N/m^2, $\mu = 1.46 \times 10^{10}$ N/m^2, and $\rho = 2400$ kg/m^3. It is represented by the subdomain $\Omega^{(1)}$ which is a cube of dimensions 1 m $\times$ 1 m $\times$ 1 m and will be discretized by 216 trilinear finite elements of size $h^{(1)} = 1/6$ m. The top surface of the foundation is subject to a uniform vertical load of magnitude 1.0 N/m^2 which varies as a unit step in time.

The halfspace $\{\mathbf{x} \in \mathbb{R}^3 : x_3 > 0\}$ is numerically represented by the surface patch $\Gamma^{(2)}$ of dimensions 5 m $\times$ 2 m which is discretized by 320 boundary elements of size $h^{(2)} = 1/4$ m. The material of this halfspace is soil with $\lambda = \mu = 1.36 \times 10^8$ N/m^2 and $\rho = 1884$ kg/m^3.

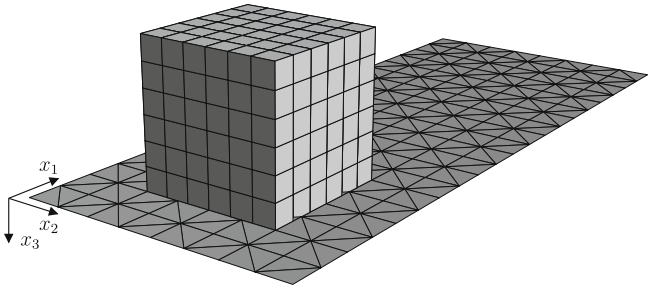

Fig. 7. Discretization of a foundation on an elastic halfspace.

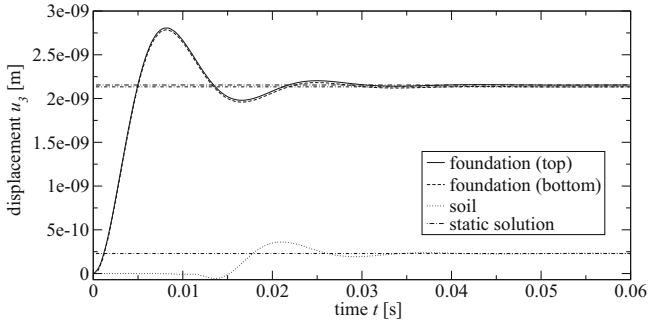

Fig. 8. Vertical displacements of the foundation and the soil against time.

The constellation of the discretizations of the foundation and the halfspace is shown in Fig. 7. In the dynamic analysis, 400 steps of size $\Delta t = 1.5 \times 10^{-4}$ s are computed. In Fig. 8, the vertical displacements at three different positions are plotted, at the midpoints of the top and bottom surfaces of the foundation and at another point on the surface of the soil. With respect to the coordinate system in Fig. 7, these points have the coordinates (1 m,1 m, – 1 m), (1 m,1 m,0), and (4.5 m,1 m,0), respectively. For these three positions the corresponding static result is given by the horizontal lines. Clearly, the static solution is reached after approximately half the computed time which indicates that the waves have been absorbed due to the infinite geometry of the elastic halfspace. Considering the point on the surface of the soil, one can see that the pressure wave is arriving after approximately 0.01 s, followed by the shear wave and the Rayleigh surface waves (cf. [1] for these wave types). No reflections of these waves occur due to the truncated surface mesh.

6. Conclusion

A framework for the coupling of finite and boundary element discretizations of dynamic and static problems has been established which allows for non-conforming interface discretizations. Basically, the concepts of hybrid domain decomposition methods [27] have been transferred to the treatment of dynamic problems, where the key point is the realization of Dirichlet-to-Neumann maps by the chosen discretization methods in time domain. In fact, the presented algorithm falls in the category of FETI/BETI methods (see [18]) but with the extension to dynamic problems and non-conforming interface discretizations. The performance in terms of the quality of the results is good both for the analysis of static and dynamic problems. Nevertheless, a further improvement can be expected if a symmetric Galerkin boundary element formulation is used in order to obtain symmetric positive system matrices throughout each step and, therefore, the use of preconditioned projected conjugate gradient solvers becomes feasible.

Acknowledgement

The second author gratefully acknowledges the financial support by the Austrian Science Fund (FWF) under grant P18481-N13.

References

[1] J. Achenbach, Wave Propagation in Elastic Solids, North-Holland, 2005.
[2] H. Bavestrello, P. Avery, C. Farhat, Incorporation of linear multipoint constraints in domain-decomposition-based iterative solvers – Part II: Blending FETI–DP and mortar methods and assembling floating substructures, Comput. Methods Appl. Mech. Engrg. 196 (2007) 1347–1368.
[3] G. Beer, Programming the Boundary Element Method: An Introduction for Engineers, Wiley, 2001.
[4] M. Costabel, Time-dependent problems with the boundary integral equation method, in: Encyclopedia of Computational Mechanics, John Wiley & Sons, Ltd., 2004, pp. 703–721.
[5] O. Estorff, C. Hagen, Iterative coupling of FEM and BEM in 3D transient elastodynamics, Eng. Anal. Boundary Elements 29 (2005) 775–787.
[6] C. Farhat, L. Crivelli, A transient FETI methodology for large-scale parallel implicit computations in structural mechanics, Int. J. Numer. Methods Engrg. 37 (1994) 1945–1975.
[7] C. Farhat, M. Géradin, On the general solution by a direct method of a large-scale singular system of linear equations: application to the analysis of floating structures, Int. J. Numer. Methods Engrg. 41 (1998) 675–696.
[8] C. Farhat, F.-X. Roux, A method of finite element tearing and interconnecting and its parallel solution algorithm, Int. J. Numer. Methods Engrg. 32 (1991) 1205–1227.
[9] C. Farhat, F.-X. Roux, Implicit parallel processing in structural mechanics, Comput. Mech. Adv. 2 (1994) 1–124.
[10] M. Fischer, L. Gaul, Fast BEM–FEM Mortar coupling for acoustic-structure interaction, Int. J. Numer. Methods Engrg. 62 (2005) 1677–1690.
[11] J. González, K. Park, C. Felippa, FEM and BEM coupling in elastostatics using localized Lagrange multipliers, Int. J. Numer. Methods Engrg. 69 (2007) 2058–2074.
[12] J. González, K. Park, C. Felippa, R. Abascal, A formulation based on localized Lagrange multipliers for BEM–FEM coupling in contact problems, Comput. Methods Appl. Mech. Engrg. 197 (2008) 623–640.
[13] F. Hartmann, Introduction to Boundary Elements. Theory and Applications, Springer, 1989.
[14] G. Hsiao, The coupling of boundary and finite element methods, Zeitschrift für angewandte Mathematik und Mechanik 70 (1990) T493–503.
[15] G. Hsiao, W. Wendland, Boundary element methods: Foundation and error analysis, in: E. Stein, R. de Borst, T. Hughes (Eds.), Encyclopedia of Computational Mechanics, vol. 1, John Wiley & Sons, Ltd., 2004, pp. 339–373 (Chapter 12).
[16] T. Hughes, The Finite Element Method: Linear Static and Dynamic Finite Element Analysis, Dover Publications, New York, 2000.
[17] A. Klawonn, O. Rheinbach, Robust FETI–DP methods for heterogeneous three dimensional elasticity problems, Comput. Methods Appl. Mech. Engrg. 196 (2007) 1400–1414.
[18] U. Langer, O. Steinbach, Coupled finite and boundary element domain decomposition methods, in: M. Schanz, O. Steinbach (Eds.), Boundary Element Analysis – Mathematical Aspects and Applications, vol. 29 of Lecture Notes in Applied and Computational Mechanics, Springer, 2007, pp. 61–95.
[19] A. Love, Treatise on the Mathematical Theory of Elasticity, Dover Publications, 1944.
[20] C. Lubich, Convolution quadrature and discretized operational calculus I&II, Numer. Math. 52 (1988) 129–145 & 413–425.
[21] W. Mansur, A Time-stepping Technique to Solve Wave Propagation Problems using the Boundary Element Method, Ph.D. thesis, University of Southampton, 1983.
[22] N. Newmark, A method of computation for structural dynamics, ASCE J. Engrg. Mech. Div. 85 (1959) 67–93.
[23] T. Rüberg, Non-conforming FEM/BEM Coupling in Time Domain, vol. 3 of Computation in Engineering and Science, Verlag der Technischen Universität Graz, 2008.
[24] M. Schanz, Wave propagation in Viscoelastic and Poroelastic Continua – A boundary element approach, Springer, 2001.
[25] D. Stefanica, Parallel FETI algorithms for mortars, Applied Numerical Mathematics 54 (2005) 266–279.
[26] O. Steinbach, Mixed approximations for boundary elements, SIAM J. Numer. Anal. 38 (2000) 401–413.
[27] O. Steinbach, Stability Estimates for Hybrid Domain Decomposition Methods, Springer, 2003.
[28] O. Steinbach, Numerical Approximation Methods for Elliptic Boundary Value Problems, Springer, 2008.
[29] E. Stephan, Coupling of boundary element methods and finite element methods, in: E. Stein, R. de Borst, T. Hughes (Eds.), Encyclopedia of Computational Mechanics, vol. 1, John Wiley & Sons, Ltd., 2004, pp. 375–412 (Chapter 13).
[30] B. Vatti, A generic solution to polygon clipping, Commun. ACM 35 (1992) 56–63.
[31] B. Wohlmuth, Discretization Methods and Iterative Solvers Based on Domain Decomposition, Springer, 2001.
[32] O. Zienkiewicz, D. Kelly, P. Bettess, The coupling of the finite element method and boundary solution procedures, Int. J. Numer. Methods Engrg. 11 (1977) 355–375.